T. BONČINA*, F. ZUPANIČ*#

IN SITU TEM STUDY OF PRECIPITATION IN A QUASICRYSTAL-STRENGTHENED Al-ALLOY

Precipitation kinetics and mechanisms within an Al-Mn-Be-Cu quasicrystal strengthened alloy at 300°C were studied using in-situ transmission electron microscopy. The alloy was cast into a copper mould. Quasicrystalline precipitates formed throughout the Al-rich solid solution, whilst heterogeneous formations of Al_2Cu and T-phase occurred on icosahedral quasicrystalline particles formed during solidification. The formation of quasicrystalline particles and T-phase was limited by manganese diffusivity, whilst that of Al_2Cu by copper diffusivity. The precipitation produced only a small hardening effect.

Keywords: precipitation, Al-alloy, transmission electron microscopy (TEM), quasicrystal

1. Introduction

Quasicrystal-strengthened Al-alloys can possess excellent combinations of strength and ductility [1]. The icosahedral quasicrystalline phases (IQCs) within these alloys are generally metastable, thus, these alloys have to be fabricated by rapid solidification [2]. However, the IQC can form at much slower cooling rates in some alloys; e.g. Al-Mn-Be, Al-Mn-Ce, Al-Mn-Fe [3-6]. The strengths of these alloys can be very high in the as-cast state [1,7]. In some alloys, the strength can be enhanced by an appropriate heat treatment. In Al-Mn-Be-Cu alloys the hardness can even be increased by 50% in comparison with the as-cast state [8]. The strongest effect can be achieved within the rapidly solidified alloys because of the high supersaturation with alloying elements in the as-cast state and as a consequence of high precipitate density after heat treatment.

Recently, in situ transmission electron microscopy (TEM) studies have become an important tool for elucidating the mechanisms and kinetics of phase transformations, despite the conditions regarding the heat treatments of thin foils and bulk samples not necessarily being the same. For example, the surface diffusion may accelerate processes in thin foils. Some of the studies have produced important results. For instance, Raskova et al. [9] studied the microstructural evolution of Al_2Cu precipitates within an ultrafine-grained Al-3wt.% Cu model alloy produced by high-pressure torsion (HPT) within the temperature range of 120°C to 170°C. They found that grain boundary diffusion was the relevant mechanism for Al_2Cu growth. Gao et al. [10] studied the precipitation behaviour of topologically close-packed (TCP) phases at an elevated temperature within a Ru-free and Ru-containing Ni-base single crystal. It was revealed that TCP phases nucleate homogeneously in the matrix and have an ori-entation relationship with the matrix. Shrestha et al. [11] found that clustering impeded the movement of dislocations during aging.

In our previous work, the effect of temperature was studied on the precipitation within an Al-Mn-Be-Cu alloy that was cast at a moderate cooling rate of about 1000 K s^{-1} [12]. It was revealed that different types of precipitates can form: θ'-Al_2Cu, IQC and T-phase. The preliminary studies showed that those processes at 200°C were too sluggish, and those at 400°C were too fast to enable and justify in-situ TEM-studies, thus the processes were studied in detail at 300°C. The aim of this presented investigation was to obtain a closer insight into processes taking place regarding isothermal holding at 300°C, and for elucidating the precipitation kinetics and mechanisms of quasicrystalline precipitates. This had not been done for quasicrystal-strengthened alloys to date. The results of this study could provide better understanding of these types of the alloys and allow better control of precipitation processes for obtaining desired combinations of mechanical properties.

2. Experimental

The alloy was vacuum induction melted using commercial master alloys, and technically pure Al. It was cast into a copper mould: $100 \times 10 \times 1$ mm. The cooling rates were about 1000 K/s. The chemical composition of the castings was determined using the atomic emission spectroscopy (AES). The alloy was composed of 4.28 wt% Mn, 0.64 wt% Be, 4.64 wt% Cu and the remainder was Al. TEM lamellas were prepared using focussed ion beam FIB (FEI, Helios) for the as-cast state. The thicknesses of lamellas were around 50 nm, and was measured from the high-

*   UNIVERSITY OF MARIBOR, FACULTY OF MECHANICAL ENGINEERING, MARIBOR, SLOVENIA

\#   Corresponding author: franc.zupanic@um.si

resolution scanning electron images. The lamellas were studied in the as-cast state using high-resolution TEM (HRTEM), energy-filtered TEM (EFTEM), scanning TEM (STEM), and energy-dispersive X-ray spectroscopy (EDXS) using FEI Titan 80-300. The in-situ study was carried out at 300°C. The heating time was about 2 minutes. The precipitate density was studied within the volume of 1000 nm × 1000 nm × 50 nm. TEM-micrographs were taken after different times. Afterwards, the number of particles were counted, and the precipitate densities were calculated.

A set of samples was heat-treated by direct artificial aging (T5-treatment) within the air. The holding times at 300°C were 15 minutes, 30 minutes, 60 minutes, 2 hours, 4 hours, 8 hours and 24 hours, and then the samples were quenched in water. The as-cast specimen and specimen heat-treated for 24 hours at 300°C were investigated by X-ray diffraction (XRD) using synchrotron X-rays with a wavelength close to 0.1 nm (Sincrotrone Elettra, Trieste, Italy). The Fisher-scope H100C micro-indentation tester was used for determining the indentation Vickers hardness under a load of 100 mN.

3. Results and discussion

Fig. 1 shows XRD-patterns of the alloy in the as-cast state and after heat treatment for 24 hours at 300°C. There were no obvious differences between both patterns. The alloy consisted of an aluminium-rich solid solution Al_{ss}, θ-Al_2Cu and icosahedral quasicrystalline phase (Table 1). Their lattice parameters were close to those in the pdf-files for FCC-Al: $a = 0.405$ nm (pdf 89-2837) and tetragonal Al_2Cu: $a = 0.6060$ nm, $c = 0.4850$ nm (pdf 65-2695).

TABLE 1

The phases identified by XRD in the as-cast state and after heat treatment at 300°C for 24 h

Phase	As-cast state	300°C, 24 h
Al_{ss}	$a = 0.40306 \pm 0.00262$ nm	$a = 0.40338 \pm 0.00159$ nm
Al_2Cu	$a = 0.60403 \pm 0.00097$ nm $c = 0.48557 \pm 0.00013$ nm	$a = 0.60449 \pm 0.00162$ nm $c = 0.48274 \pm 0.00081$ nm
IQC	*present*	*present*

Fig. 2 shows a typical microstructure after heat treatment at 300°C for 1 hour, which was apparently the same as the microstructure in the as-cast state. The microstructure was composed of the dark dendritic Al_{ss}, binary eutectic ($Al_2Cu + Al_{ss}$), primary icosahedral phase and binary eutectic (IQC + Al_{ss}). At this magnification, no precipitates were observed in the matrix, however, nanosized IQC-precipitates were revealed by a TEM investigation.

Fig. 3 and 4 contain TEM-micrographs of the investigated area after different holding times at 300°C. The TEM-lamella from the as-cast sample was cut from a region similar to that indicated by the rectangle in Fig. 2. The micrographs in Fig. 3 were taken with a high-angle annular dark field detector (HAADF) in the STEM-mode. The brighter regions indicate those phases
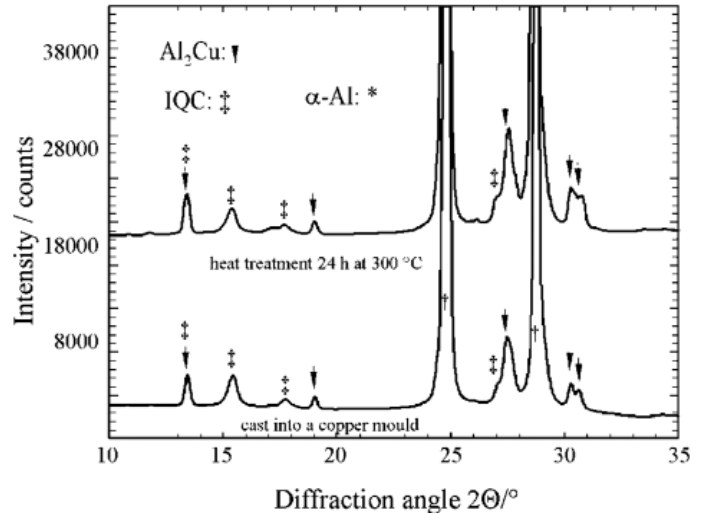

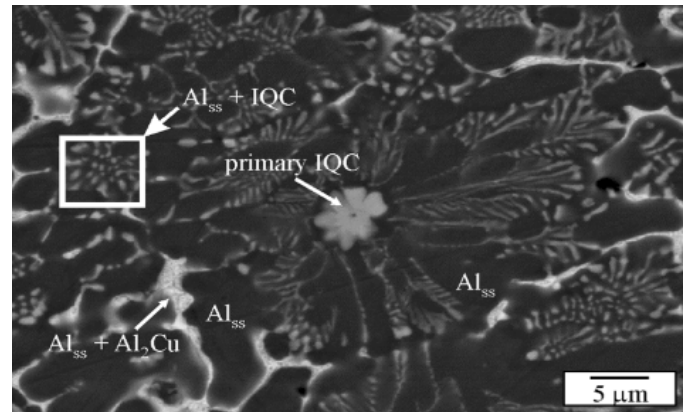Fig. 1. XRD-patterns of the alloy in the as-cast state and after heat treatment at 300°C for 24 hours

Fig. 2. Backscattered electron micrograph of the alloy after 1h heat treatment at 300°C. A TEM-lamella from the sample in the as-cast state was cut from an area similar to that indicated by the rectangle
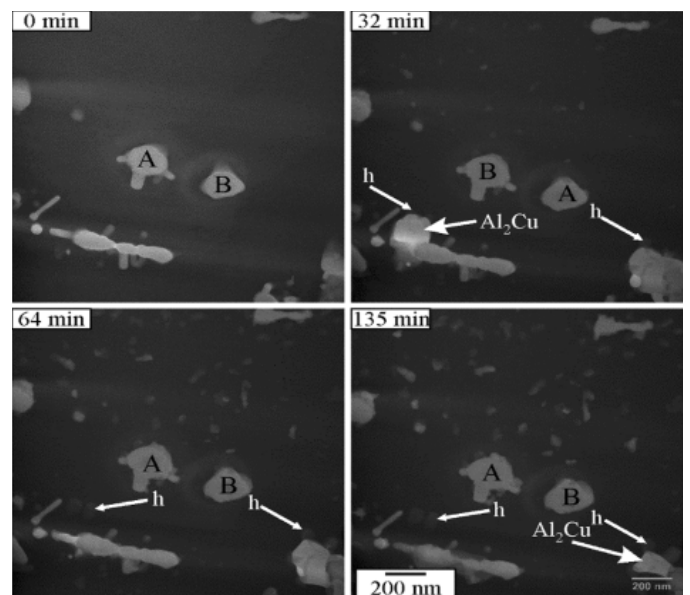

Fig. 3. STEM-HAADF micrographs after different holding times at 300°C

containing heavier atoms; they contained Mn and/or Cu within this alloy. The micrographs in Fig. 4 were taken using EFTEM that allowed acquisition of the elemental maps for Cu and Mn but not of Be. These maps make the identification of phases much easier. The two primary IQC particles indicated by A and B are marked within all micrographs. No microstructural changes were noticed during 2-minutes heating from room temperature to 300°C. Afterwards, three distinct processes were observed: (1) the formation and growth of precipitates within the Al_{ss}-matrix; (2) the nucleation and growth of particles on the IQC that were present within the as-cast condition, and (3) the formation, growth and dissolution of Al_2Cu.
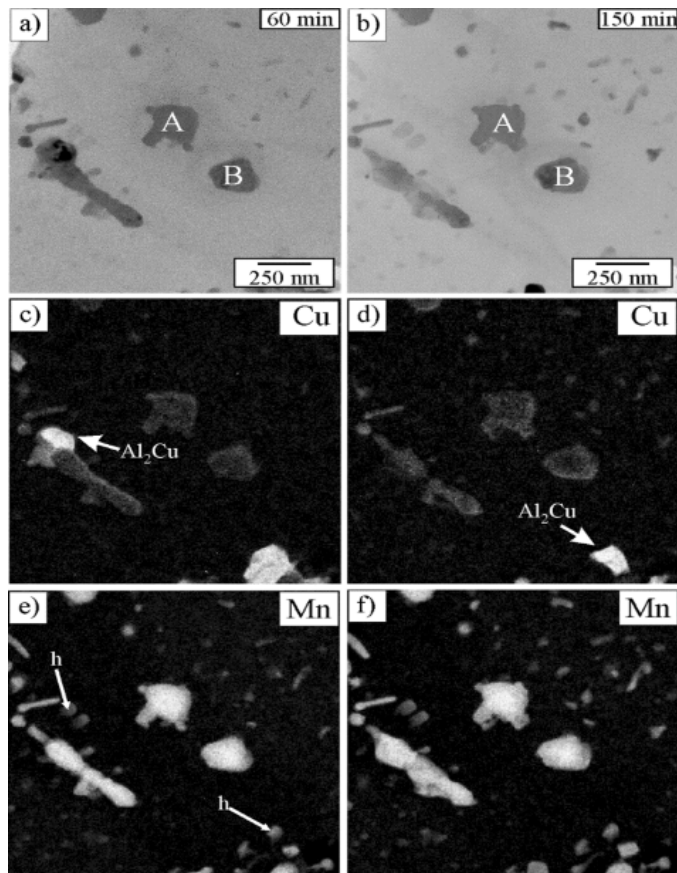

Fig. 4. In-situ treatment at 300°C for 60 and 150 min. a, b) TEM bright-field image, c, d) EFTEM distributions of Cu, and e, f) EFTEM distributions of Mn

3.1. Precipitation within the Al_{ss}

The precipitates formed within Al_{ss} grains were detected when their diameters reached about 10 nm. The cumulative number of particles is given in Fig. 5a. The incubation period under these circumstances was about 10 minutes. The nucleation rates were calculated from the particle count after different holding times (Fig. 5b). The nucleation rate started to increase considerably after 15 minutes, and attained the maximum value of around 10^{18} m^{-3} s^{-1} after 20 minutes at 300°C. The nucleation rate dropped by almost two orders of magnitude after 30 minutes, and the formation of new precipitates apparently stopped after 60 minutes. Thereafter, only growth of the existing precipitates took place. Some precipitates thickened uniformly whilst others became elongated. No precipitate ripening was observed during the observation.

Fig. 4a and 4b show the investigated area after 60 minutes and 150 minutes at 300°C. The corresponding EFTEM-maps for Cu and Mn showed that precipitates contained both Cu and Mn, whilst Be was undetected using this method. The content of Mn was higher than that of Cu. The Cu-content within the precipitates seemed to be almost the same as in the primary IQC-particles; within the range of few atomic percentages. The calculated root-mean-square (RMS) diffusion distances for Cu and Mn at this temperature for different times are collated in Table 2. The precipitate sizes and the interparticle distances were comparable with the RMS distances for Mn, indicating that Mn-diffusion limits the formation and growth of precipitates. The interparticle distances and precipitate sizes were slightly larger than the RMS distances for Mn, which can be caused by the presence of quenched-in vacancies and partly the enhanced surface diffusion.

After cooling the sample back to room temperature, HR-TEM images were acquired for studying the structures of the precipitates. Fig 6 shows a HRTEM-image of the IQC-precipitate within the matrix Al_{ss} and corresponding FFTs. The threefold axis of Al_{ss} [11$\bar{1}$] was parallel to the threefold axis of IQC: [τ^{-2} 1 0]. Closer inspection showed an excellent matching between the matrix and the precipitate and by coincidence some diffraction spots within the corresponding FFTs. The lattice planes extended epitaxially from the quasi-crystalline phase to the FCC-matrix.
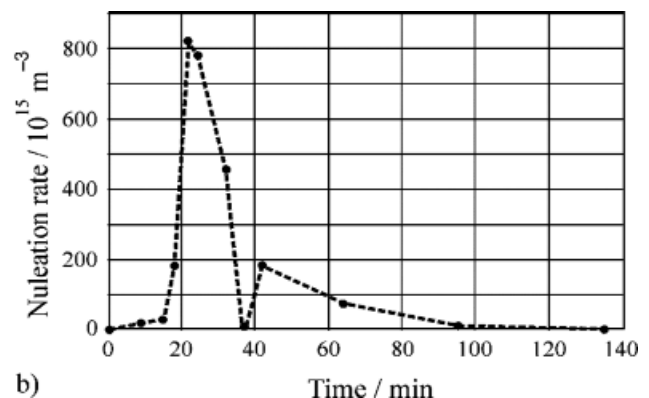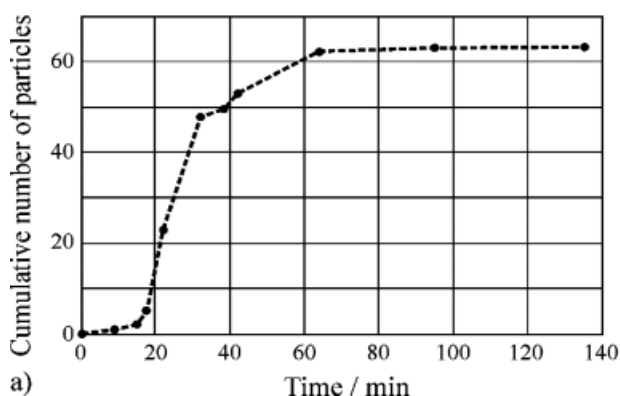

Fig. 5. Precipitates in the matrix: a) cumulative number of particles, and b) the nucleation rate as a function of time

Similar results were found at interfaces between IQC and different crystalline phases [13]. This allowed the creation of a low energy interface between IQC and Al$_{ss}$, which decreased the nucleation barrier and facilitated the formation of IQC-precipitates. The precipitate density was around 5×10^{13} m^{-2}. This was much higher than expected for the dislocation density in the as-cast state; e.g. the dislocation density should be within the range of 10^{10} m^{-2}. According to this, it can be assumed that the IQC-precipitates mainly formed homogeneously within the matrix.

The microindentation study revealed the samples heat-treated at 300°C exhibited maximum hardness after approximately 60 minutes, which coincided with the ceasing of precipitation formation during the in-situ TEM study. The hardness increased from 120 HV in the as-cast state to 135 HV after 60 minutes. The hardening effect was not too strong in this case.
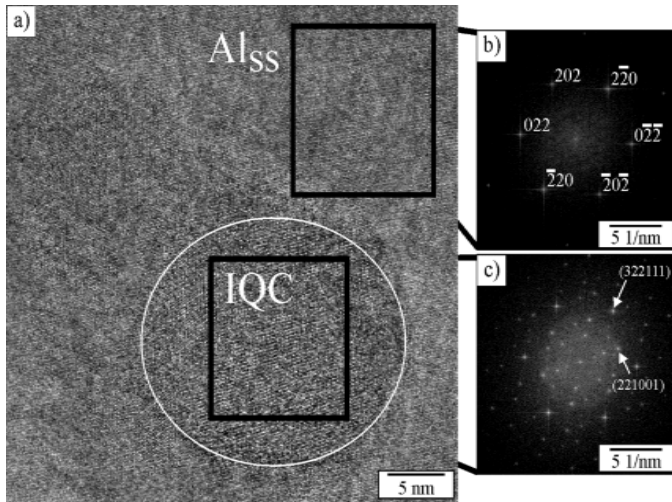

Fig. 6. The HRTEM micrograph of an IQC-precipitate (encircled) within Al$_{ss}$ with corresponding FFTs for the matrix (zone axis [111]), and IQC-precipitate (a threefold zone axis [τ^{-2} 1 0]

3.2. Precipitates on the IQC formed during solidification

The IQC-particles formed during solidification represented heterogeneous nucleation sites for other types of precipitates. Several other precipitates formed on each IQC-particle (Fig. 7). The first precipitates started to form around 15 minutes after heating to 300°C. Their initial sizes were about 15 nm in length l (parallel to the IQC/α-Al interface) and 10 nm in thickness h (perpendicular to the IQC/α-Al interface). The lengthening proceeded as approximately linear with time and the thickening was roughly proportional to $t^{0.5}$ (t is time). After 150 minutes the lengths of the precipitates were up to 135 nm and the thicknesses up to 50 nm.

Fig. 8a shows an image of a smaller precipitate that formed at the interface between primary IQC and Al$_{ss}$. The FFT of the precipitate exhibited periodicity, with a rectangular lattice (Fig. 8b). The smallest reciprocal lattice vectors were perpendicular to each other, and their lengths were about 0.83 nm^{-1}

and 0.79 nm^{-1}, corresponding to interplanar lattice spacings of 1.20 nm and 1.26 nm, respectively. These values corresponded to crystallographic planes (200) and (010) of the T-phase, which was found to precipitate within Al$_{ss}$ at 400°C and 500°C [12]. The zone axis of the T-precipitate was [001]. Two typical diffraction spots (10 3 0) and (060) are indicated in Fig. 8b.

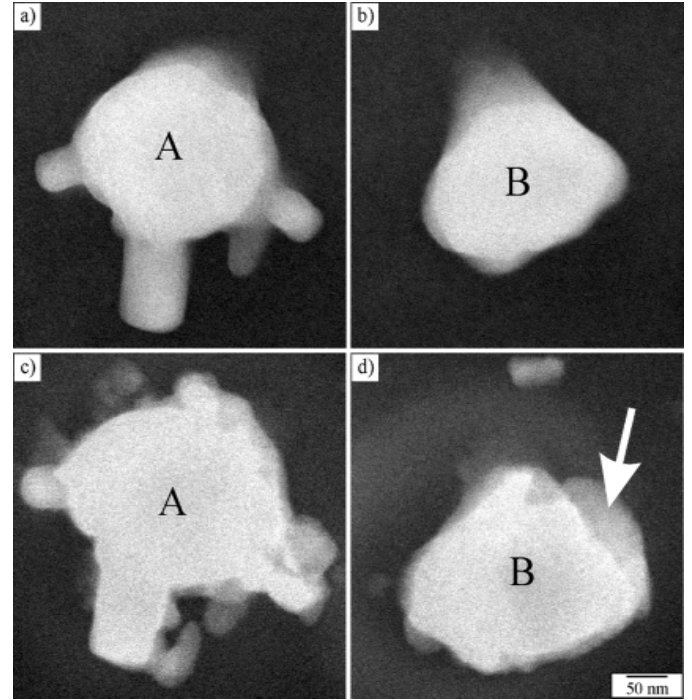
Fig. 7. HAADF-micrographs of precipitates formed on the IQC-particles: a, b) just heated to 300°C, c, d) after 135min at 300°C
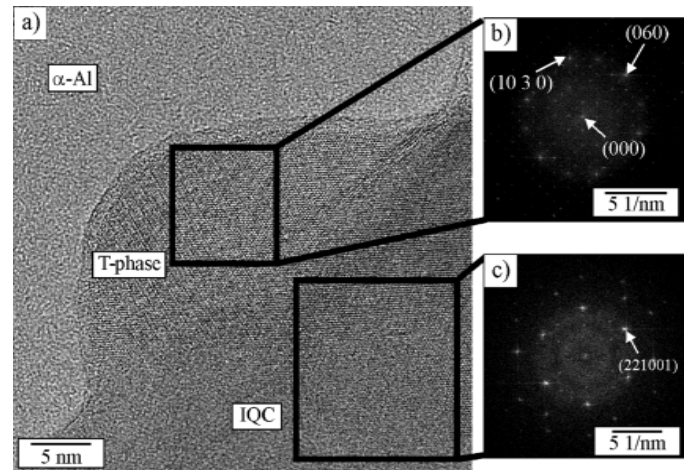

Fig. 8. The nucleation of IQC: a) HRTEM of a T-phase precipitate formed on IQC, b) its corresponding FFT along [001] zone axis, c) FFT of the IQC along its threefold axis [τ^{-2} 1 0]

3.3. Behaviour of θ-Al$_2$Cu

The Θ-Al$_2$Cu was absent within the investigated region in the as-cast microstructure. All Θ-Al$_2$Cu started to appear several minutes after heating to 300°C, and all had appeared within a very short time period. Θ-Al$_2$Cu nucleated on IQC eu-

tectic branches and grew during the first 15 minutes of holding. Afterwards they started to dissolve linearly over time. Almost all Al$_2$Cu had dissolved after 60 minutes, only some remains of Al$_2$Cu particles persisted within the microstructure after 150 minutes (e.g. the particle indicated by the arrow in Fig. 4b).

The root-mean-square (RMS) diffusion distances for Cu were within the range of a few 100 nm, which were about 200-times larger than the RMS diffusion distances for Mn (Table 2). Thus, copper atoms could aggregate from the much larger region. The supersaturation of the matrix with Cu obtained by non-equilibrium solidification could be accomplished by the formation of Al-Cu phases. The temperature of 300°C lies above the metastable solvus temperatures for GP-zones, θ''- and θ'-precipitates, thus only Θ-Al$_2$Cu can form. As the crystal structure of Θ-Al$_2$Cu considerably differs from that of Al$_{ss}$, the heterogeneous nucleation prevailed, as in binary Al-Cu alloys. The IQC eutectic branches represented convenient nucleation sites. The T-phase that formed on the IQC eutectic branches contained ≈8 at.% Cu, thus this phase becomes a sink for Cu atoms. A previous study showed that the T-phase is more stable than Al$_2$Cu [14], thus the content of Cu at the T/Al$_{ss}$ interphase was smaller than at the Θ/Al$_{ss}$ interphase. This caused diffusion of Cu from Θ/Al$_{ss}$ to T/Al$_{ss}$, and dissolution of Al$_2$Cu.

The dynamic behaviour of Θ-Al$_2$Cu also made possible the heterogeneous formation of precipitates – probably of T-phase. These are precipitates assigned with "h" in Fig. 3 and 4. These precipitates were growing whilst θ-Al$_2$Cu was dissolving. The shape of precipitates strongly resembled that of the T-phase. Unfortunately, we failed to obtain satisfactory HRTEM-images for determining their structures.

In the meantime it also served as a heterogeneous nucleation site for precipitates, probably of the T-phase. The precipitation did not produce significant strengthening. An important task for further investigations lies in optimisation of the chemical composition to produce higher supersaturation with alloying elements in the matrix at moderate cooling rates, in order to provide stronger strengthening effect.

TABLE 2

The root-mean-square (RMS) diffusion distances $\sqrt{4Dt}$ for Cu and Mn at 300°C with increasing holding time

t / min	RMS for Cu at 300°C /nm $D = 2.6 \times 10^{-17}$ m^2 s^{-1} [15]	RMS for Mn at 300°C /nm $D = 7 \times 10^{-22}$ m^2 s^{-1} [15]
15	306	1.6
30	433	2.2
60	613	3.17
120	867	4.5
150	969	5

4. Conclusions

The in-situ TEM study of the quasicrystal-strengthened Al-alloy enabled determination of the mechanisms and kinetics of several processes at 300°C. The IQC-precipitates formed within the matrix Al$_{ss}$ during the first 60 minutes, and afterwards they only grew. The IQC eutectic branches presented convenient heterogeneous nucleation sites for the T-phase precipitates. The θ-Al$_2$Cu was very dynamic. Firstly, it formed heterogeneously on the IQC eutectic branches, then grew, and finally dissolved.

REFERENCES

[1] A. Inoue, H. Kimura, Current Opinion in Solid State and Materials Science **2**, 305 (1997).

[2] F. Schurack, J. Eckert, L. Schultz, Acta Mater. **49**, 1351 (2001).

[3] K.B. Kim, W. Xu, M. Tomut, M. Stoica, M. Calin, S. Yi, W. H. Lee, J. Eckert, J. Alloy. Compd. **436**, L1 (2007).

[4] S.H. Kim, G.S. Song, E. Fleury, K. Chattopadhyay, W.T. Kim, D.H. Kim, Philosophical Magazine a-Physics of Condensed Matter Structure Defects and Mechanical Properties **82**, 1495 (2002).

[5] F. Schurack, J. Eckert, L. Schultz, Philos. Mag. **83**, 807 (2003).

[6] T. Boncina, B. Markoli, F. Zupanic, J. Microsc.-Oxf. **233**, 364 (2009).

[7] N. Rozman, T. Boncina, I. Anzel, F. Zupanic, Mater. Tehnol. **42**, 65 (2008).

[8] F. Zupanic, G. Lojen, L. Barba, T. Boncina, Mater. Charact. **70**, 48 (2012).

[9] B. Rashkova, M. Faller, R. Pippan, G. Dehm, J. Alloy. Compd. **600**, 43 (2014).

[10] S. Gao, Y.Z. Zhou, C.F. Li, J.P. Cui, Z.Q. Liu, T. Jin, J. Alloy. Compd. **610**, 589 (2014).

[11] S.L. Shrestha, K.Y. Xie, S.P. Ringer, K.R. Carpenter, D.R. Smith, C.R. Killmore, J.M. Cairney, Scripta Materialia **69**, 481 (2013).

[12] F. Zupanič, D. Wang, C. Gspan, T. Bončina, Mater. Charact. **106**, 93 (2015).

[13] A. Singh, A. P. Tsai, J. Phys.-Condes. Matter **20** (2008).

[14] F. Zupanic, T. Boncina, J. Alloy. Compd. **617**, 174 (2014).

[15] Y. Du, Y.A. Chang, B.Y. Huang, W.P. Gong, Z.P. Jin, H.H. Xu, Z.H. Yuan, Y. Liu, Y.H. He, F.Y. Xie, Mater. Sci. Eng. A-Struct. Mater. Prop. Microstruct. Process. **363**, 140 (2003).